



SHORT COMMUNICATION



Donepezil + chromone + melatonin hybrids as promising agents for Alzheimer's disease therapy

Irene Pachón-Angona^a, Bernard Refouvelet^a, Rudolf Andrys^b, Helène Martin^c, Vincent Luzet^a, Isabel Iriepa^{d,e}, Ignacio Moraleda^d, Daniel Diez-Iriepa^{d,e}, María-Jesús Oset-Gasque^{f,g}, José Marco-Contelles^h, Kamil Musilek^b  and Lhassane Ismaili^a 

^aNeurosciences intégratives et cliniques, Pôle Chimie Organique et Thérapeutique, University Bourgogne Franche-Comté, Besançon, France; ^bFaculty of Science, Department of Chemistry, University of Hradec Kralove, Hradec Kralove, Czech Republic; ^cPEPITE EA4267, Laboratoire de Toxicologie Cellulaire, University Bourgogne Franche-Comté, Besançon, France; ^dDepartment of Organic Chemistry and Inorganic Chemistry, Alcalá University, Madrid, Spain; ^eInstitute of Chemical Research Andrés M. del Río, Alcalá University, Madrid, Spain; ^fInstituto de Investigación en Neuroquímica, Universidad Complutense de Madrid, Madrid, Spain; ^gDepartment of Biochemistry and Molecular Biology, School of Pharmacy, Plaza de Ramón y Cajal, Madrid, Spain; ^hLaboratory of Medicinal Chemistry (IQOG, CSIC), Madrid, Spain

ABSTRACT

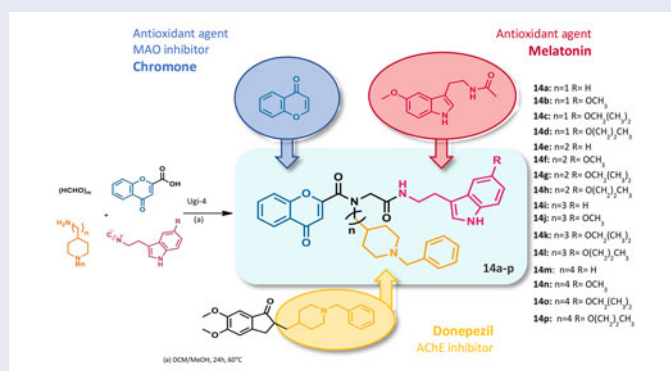
We describe herein the design, multicomponent synthesis and biological studies of new donepezil + chromone + melatonin hybrids as potential agents for Alzheimer's disease (AD) therapy. We have identified compound **14n** as promising multitarget small molecule showing strong BuChE inhibition ($IC_{50} = 11.90 \pm 0.05$ nM), moderate hAChE ($IC_{50} = 1.73 \pm 0.34$ μ M), hMAO A ($IC_{50} = 2.78 \pm 0.12$ μ M), and MAO B ($IC_{50} = 21.29 \pm 3.85$ μ M) inhibition, while keeping a strong antioxidant power (3.04 TE, ORAC test). Consequently, the results reported here support the development of new multitarget Donepezil + Chromone + Melatonin hybrids, such as compound **14n**, as a potential drug for AD patients cure.

ARTICLE HISTORY

Received 25 June 2018
Revised 21 October 2018
Accepted 4 November 2018

KEYWORDS

Antioxidant; cholinesterases; donepezil; MAO-A; MAO-B; ORAC; Ugi-4MCR



Introduction



Alzheimer's disease (AD) remains the most common cause of cognitive impairment in aging population¹. AD is a multifactorial disorder exhibiting highly interconnected physiopathological processes², leading to a dramatic loss of cholinergic neurons, low level of acetylcholine (ACh), accumulation of intracellular neurofibrillary tangles, abnormal extracellular deposits of amyloid β peptide ($A\beta$), associated to accumulation of biometals (Cu, Fe, Zn) and oxidative stress (OS)^{3–5}.


Based on the multifactorial nature of AD and the inadequate therapeutic efficacy of monotarget therapeutic approach, new strategies have been advanced based on the multitarget small

molecule (MTSM) approach for the development of new drugs able to bind simultaneously at diverse enzymatic systems or receptors involved in the pathology^{6–11}. Accordingly, in our laboratory, we have developed a number of new MTSM as acetylcholinesterase inhibitors (AChEIs) and strong antioxidants, prepared by multicomponent reaction (MCRs)^{12–14}.

MCRs have emerged as powerful synthetic methodologies transforming three or more starting materials into new products, in a one-pot procedure^{15,16}, being the method of choice for introducing rapidly and efficiently chemical diversity¹⁷. Therefore, they seem well-suited in the search for new MTSM.

In this paper, we report the design, synthesis and the biological evaluation of a new family of chromones resulting from

CONTACT Lhassane Ismaili  lhassane.ismaili@univ-fcomte.fr  Neurosciences intégratives et cliniques, Pôle Chimie Organique et Thérapeutique, University Bourgogne Franche-Comté, UFR Santé, 19, rue Ambroise Paré, Besançon, F-25000, France

 Supplemental data for this article can be accessed [here](#).

© 2019 The Author(s). Published by Informa UK Limited, trading as Taylor & Francis Group.

This is an Open Access article distributed under the terms of the Creative Commons Attribution License (<http://creativecommons.org/licenses/by/4.0/>), which permits unrestricted use, distribution, and reproduction in any medium, provided the original work is properly cited.

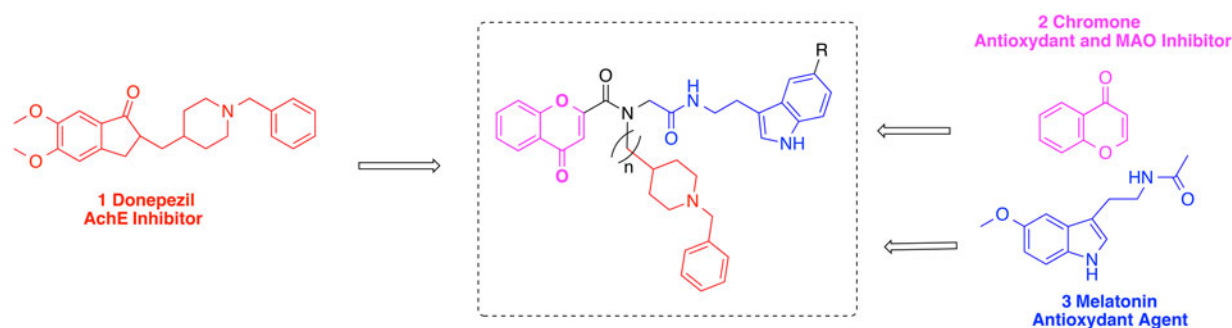


Figure 1. Design of donepezil-chromone-melatonin hybrids.

the Ugi four-MCR (Ugi-4MCR), by incorporating selected motifs from Donepezil, and Melatonin (Figure 1). Donepezil (**1**) (Figure 1), a ChE inhibitor (ChEI), was the second drug approved by the US FDA for the treatment of mild to moderate AD. Donepezil bears *N*-benzylpiperidine and indanone moieties, and exhibits selectivity for the inhibition of AChE over butyrylcholinesterase (BuChE)¹¹.

The Chromone (**2**) (Figure 1) is a privileged scaffold in medicinal chemistry, and the core fragment of several flavonoid derivatives exhibiting a wide range of pharmacological activities¹⁸, including particularly their ability to inhibit monoamine oxidase enzymes (MAO)^{19–21}. It is well known that monoamine oxidase inhibitors (MAOIs) are able to reduce the formation of neurotoxic H₂O₂ which increase the formation of reactive oxygen species (ROS)²², and have therapeutic potential for the treatment of AD and Parkinson's disease^{23,24}.

The powerful indirect antioxidant functions²⁵ of Melatonin (**3**) (Figure 1), and its ability to scavenge different types of ROS in cells²⁶, confers to this compound a strong neuroprotective capacity against OS²⁷. Melatonin plays likewise a neuroprotective role against A β ²⁸ and easily crosses the brain-blood barrier.

Lead hybridisation-based synthesis of combinational pharmacophoric groups is a new strategy in drug discovery, of paramount interest and an important starting point for the identification of new chemical entities which are likely to have improved biological activities respect to the standard ligands used as models; in addition, this drug-design approach results in ligands showing diverse selectivity profile, and modes of action minimising/minimising the secondary side effects²⁹.

Considering these precedents, and using a Ugi-4 MCR, we have designed the new MTSM of general structure **I** (Figure 1), synthesised/synthesised sixteen new hybrids **14a–p** (Scheme 1, Table 1), and evaluated their ChE and MAO inhibition, as well as their antioxidant activity (ORAC-FL test). From these studies, we have identified derivative **14n** (Scheme 1, Table 1) as new and very promising hit-MTSM for the potential AD therapy.

Methods

Chemistry

General procedure for the ugi-4MCR synthesis of compounds

A solution of the corresponding *N*-benzylpiperidines **8–11** (1.0 mmol) and paraformaldehyde (**13**) (1.0 mmol) in MeOH/CH₂Cl₂ (7 ml, 3:1, v/v) was stirred for 1 h at room temperature (rt). Chromone-2-carboxylic acid (**12**) (1.0 mmol) and the appropriate isocyanide **4–7** (1.0 mmol) were then added. The reaction was stirred 24 h at rt, and when complete (tlc control), the crude product was isolated and purified by flash column chromatography to afford the corresponding hybrids **14a–p** (see Supplementary Material).

Biological evaluation

Oxygen radical absorbance capacity assay

The antioxidant activity of hybrids **14a–p** was carried out by the ORAC-FL using fluorescein as a fluorescent probe. Briefly, fluorescein and antioxidant were incubated in a black 96-well microplate (Nunc) for 15 min at 37 °C. The 2,2'-azobis(amidinopropane) dihydrochloride was then added quickly using the built-in injector of Varioskan Flash plate reader (Thermo Scientific). The fluorescence was measured at 485 nm (excitation wavelength) and 535 nm (emission wavelength) each min for 1 h^{30,31}.

MAO activity assay

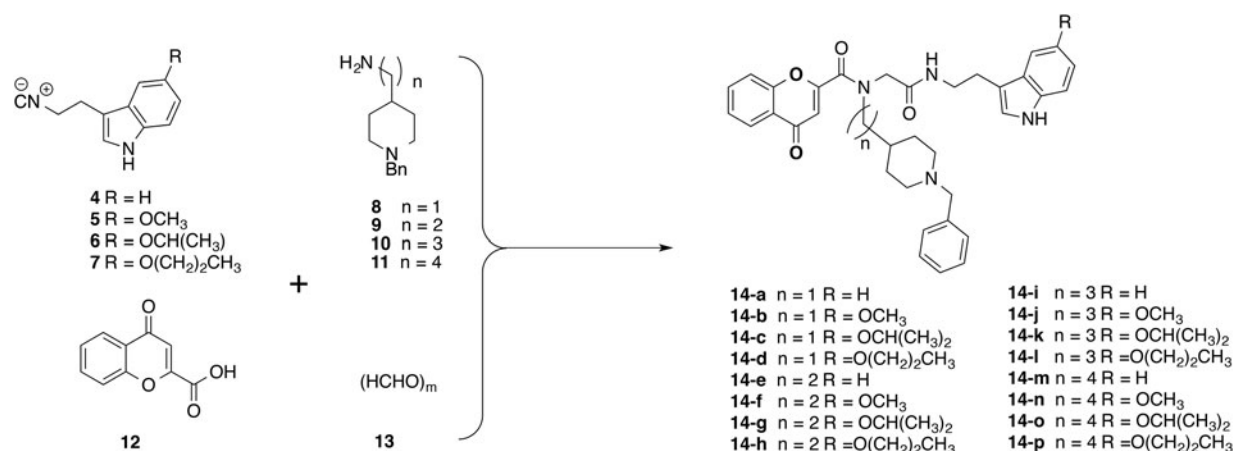
The reaction mixture contains 2.5 μ g/mL MAO-A or 6.25 μ g/mL MAO-B enzyme and inhibitor in final concentrations of 1, 5, 8, 10, 15, 30, 50, and 80 μ M in 50 mM potassium phosphate buffer with 20% (v/v) glycerol (pH 7.5). The mixture was pre-incubated at 37 °C for 5 min and subsequently, substrate kynuramine was added to the final concentration of 60 μ M in case of MAO-A and 30 μ M in case of MAO-B. The final volume of reaction mixture was 0.1 ml. The whole reaction mixture was incubated at 37 °C for 30 min. The reaction was stopped by the addition of 200 μ l acetonitrile:methanol mixture (ratio 1:1) and cooling down to 0 °C. The sample was then centrifuged (16,500 g) for 10 min.

Metabolite determination

The deamination product of kynuramine formed during the enzymatic reaction 4-hydroxyquinoline (4-HQ) was determined by HPLC–MS on a 2.1 mm \times 50 mm, 1.8 μ m Zorbax RRHD Eclipse plus C18 column (Agilent), by using an 6470 Series Triple Quadrupole mass spectrometer (Agilent) (electrospray ionisation - positive ion mode). Three m/z MRM transitions were followed for kynuramine (165.1=>30.2, 165.1=>118.0, 165.1=>136.0) and 4-HQ (146.1=>51.1, 146.1=>77.0, 146.1=>91.0). Eluents: (A) 0.1% formic acid in water; (B) 0.1% formic acid in acetonitrile. IC₅₀ of individual compounds were determined using GraphPad Prism 6.0, San Diego, CA.

ChE activity assay

Inhibition of *Ee*AChE and eqBuChE of hybrids **14a–p** was carried out with *Ee*AChE (type VI-S, purified from *Electrophorus electricus*) and eqBuChE (purified from equine serum) using Ellman's protocol³². Briefly, the reaction was performed in a final volume of 3 ml of a phosphate-buffered solution (0.1 M) at pH = 8.0 containing 5,5'-dithiobis-2-nitrobenzoic acid (DTNB) (2.625 μ L, 0.35 mM), *Ee*AChE (29 μ L, 0.035 U/mL) or eqBuChE (60 μ L, 0.05 U/mL), Bovine Albumin Serum phosphate-buffered solution (40 μ L 1% w/v), and tested compound (3 μ L). After 10 min of incubation, the substrate,



Scheme 1. Synthesis of the Donepezil-Chromone_melatonin Hybrids **14a-p**. Conditions: MeOH/CH₂Cl₂ (3:1), rt, 24 h.

Table 1. ORAC-FL values, Inhibition of *Ee*AChE, hACHE, eqBuChE, hMAOA and hMAOB values for **14a-p**, ferulic acid, melatonin, donepezil, tacrine clorgyline, and pargyline.

Ref.	n	R	ORAC ^a (Eq Trolox)	IC ₅₀ hMAO A ^b (μM)	IC ₅₀ hMAO B ^b (μM)	IC ₅₀ <i>Ee</i> AChE ^b (μM)	IC ₅₀ eqBuChE ^b (nM)	IC ₅₀ hACHE ^b (μM)	IC ₅₀ hBuChE ^b (nM)
14a	1	H	6.28 ± 0.12	2.00 ± 0.13	— ^c	— ^d	496.02 ± 7.07	— ^d	1167.30 ± 19.05
14b	1	OCH ₃	6.24 ± 0.05	— ^c	— ^c	— ^d	636.23 ± 11.64	— ^d	— ^d
14c	1	OCH(CH ₃) ₂	6.11 ± 0.07	— ^c	— ^c	— ^d	245.73 ± 9.91	— ^d	— ^d
14d	1	O(CH ₂) ₂ CH ₃	6.76 ± 0.09	— ^c	— ^a	— ^d	46.89 ± 3.41	— ^d	— ^d
14e	2	H	6.52 ± 0.37	— ^c	— ^c	1.43 ± 0.05	29.59 ± 2.38	2.62 ± 0.53	33.30 ± 0.55
14f	2	OCH ₃	6.13 ± 0.09	— ^c	80.59 ± 13.88	0.69 ± 0.03	26.03 ± 2.37	0.36 ± 0.16	271.75 ± 1.75
14g	2	OCH(CH ₃) ₂	5.05 ± 0.15	— ^c	— ^c	1.05 ± 0.06	6.29 ± 0.73	2.00 ± 0.07	25.00 ± 0.20
14h	2	O(CH ₂) ₂ CH ₃	6.07 ± 0.02	— ^c	— ^c	0.85 ± 0.02	6.76 ± 0.49	2.04 ± 0.66	63.90 ± 2.55
14i	3	H	6.92 ± 0.32	— ^c	— ^c	0.26 ± 0.01	50.11 ± 5.19	— ^d	— ^d
14j	3	OCH ₃	3.31 ± 0.10	— ^c	— ^c	0.27 ± 0.00	37.06 ± 0.46	— ^d	— ^d
14k	3	OCH(CH ₃) ₂	2.27 ± 0.37	2.99 ± 0.16	15.17 ± 2.33	0.36 ± 0.01	18.21 ± 0.18	— ^b	34.90 ± 0.85
14l	3	O(CH ₂) ₂ CH ₃	2.44 ± 0.16	— ^c	— ^c	0.38 ± 0.01	9.03 ± 0.18	— ^d	— ^d
14m	4	H	2.97 ± 0.16	— ^c	— ^c	0.06 ± 0.00	355.33 ± 8.41	— ^d	— ^d
14n	4	OCH ₃	3.04 ± 0.36	2.78 ± 0.12	21.29 ± 3.85	0.48 ± 0.01	43.38 ± 1.37	1.73 ± 0.34	11.90 ± 0.05
14o	4	OCH(CH ₃) ₂	2.63 ± 0.12	— ^c	— ^c	0.09 ± 0.00	46.62 ± 2.76	— ^d	— ^d
14p	4	O(CH ₂) ₂ CH ₃	2.67 ± 0.15	1.39 ± 0.11	— ^c	0.08 ± 0.00	61.33 ± 5.48	2.10 ± 0.51	80.35 ± 12.35
Ferulic acid	—	—	3.74 ± 0.22	— ^e	— ^e	— ^e	— ^e	— ^e	— ^e
Melatonin	—	—	2.45 ± 0.09	— ^e	— ^e	— ^e	— ^e	— ^e	— ^e
Donepezil	—	—	— ^e	— ^e	— ^e	0.02 ± 0.00	840 ± 20	0.023 ± 0.01	7420 ± 390
Tacrine	—	—	0.2 ± 0.1	— ^e	— ^e	0.03 ± 0.01	5.1 ± 0.1	0.424 ± 21 ³⁷	45.8 ± 3.0 ³⁷
Clorgyline	—	—	— ^e	0.05 ± 0.00	— ^e	— ^e	— ^e	— ^e	— ^e
Pargyline	—	—	— ^e	— ^e	0.08 ± 0.01	— ^e	— ^e	— ^e	— ^e

^aData are expressed as Trolox equivalents and are the mean (n = 3) ± SD.

^bEach IC₅₀ value is the mean ± SEM of at least three different experiments.

^cEnzymatic inhibition (%) <40% at 10 μM;

^dEnzymatic inhibition (%) <50% at 10 μM;

^enot determined.

AcTCh) iodide or butyrylthiocholine (BuTCh) iodide, was added, and the reaction was incubated for an additional 15 min. The absorbances were measured in a spectrometric plate reader at 412 nm and the IC₅₀ were determined using GraphPad Prism 5, San Diego, CA.

To investigate the inhibitory capacity of the compounds on hAChE and hBuChE, Ellman's spectrophotometric method³² was used with minor modifications³³, using recombinant expressed in HEK 293 hAChE (Sigma Aldrich, Madrid, Spain) and hBuChE from human serum (Sigma Aldrich, Madrid, Spain). The reaction was carried out in a 48-well plate at 37 °C on a final volume of 500 μL of a phosphate buffer solution (TPS 0.1 M pH 8), each well containing 200 μL of 0.875 mM of DTNB (5,5'-dithiobis -2-nitrobenzoic acid in PBS 1×) and 5 μL hAChE (CSU 3.6 U/mL) or 5 μL hBuChE (CSU 5 U/mL) for a final concentration of 0.036 U/mL or 0.05 U/mL in each well. The reaction was started by adding acetylthiocholine (AcTCh) at 0.35 mM (Cf in the well) for hAChE, and butyrylthiocholine (BuTCh) at 1 mM (Cf in the well). The enzymatic reaction was

monitored at 410 nm of absorbance during 5 min for hAChE and 8 min for hBuChE in a Biotek Power Wave XS spectrophotometer plate reader (kinetic measure each 15 s). Inhibition curves were performed by pre-incubation of this mixture with at least five concentrations of each compound (10 nM–100 μM in case of hAChE, and 10 pM–75 μM in case of hBuChE) for 10 min. A control sample (without compound) and a tacrine dilution at IC₅₀ concentration (500 nM for hAChE and 30 nM for hBuChE) were always included to determine 100% of the enzymatic activity in each assay. After this pre-incubation period, the corresponding substrate was added and put in the spectrophotometer during 5 or 8 min for the colour change detection of the enzymatic reaction.

Molecular docking of compound **14n** into hAChE and hBuChE

The structure of compound **14n** was built as its hydrochloride using standard bond lengths and bond angles with Discovery

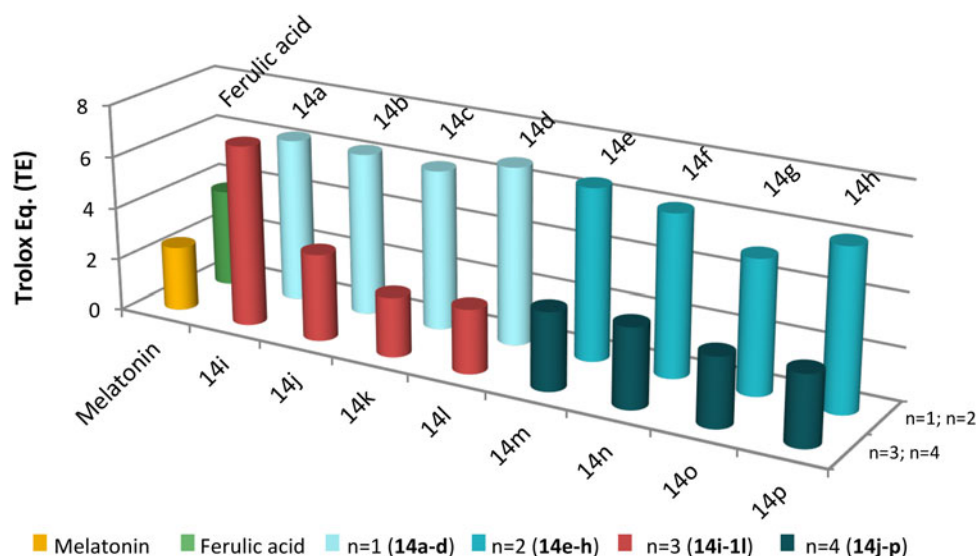


Figure 2. Antioxidant power of compounds **14a–p** compared to melatonin and ferulic acid.

Studio, version 2.1, software package, San Diego, CA. The molecular geometry of **14n** was energy-minimised with the CHARMM force field³⁴ using the adopted-based Newton–Raphson algorithm, considering this structure fully optimised when the energy changes between iterations were less than kcal(mol·Å)⁻¹³⁵. The ligand was set up for docking with the help of AutoDockTools (ADT; version 1.5.4) to define the torsional degrees of freedom to be considered during the docking process. All the acyclic dihedral angles in the ligand were allowed to rotate freely.

The enzyme structure used for the calculations was the human AChE (Protein Data Bank code 1B41). For docking purposes, the initial protein was prepared by removing all water molecules, heteroatoms, any co-crystallised solvent, and the ligand. Proper bonds, bond orders, hybridisation, and charges were assigned using protein model tool in Discovery Studio, version 2.1, software package, San Diego, CA. CHARMM force field was applied using the receptor-ligand interactions tool in Discovery Studio, version 2.1, software package. ADT was used to add hydrogens and partial charges for proteins and ligands using Gasteiger charges. To give flexibility to the binding site, residues lining the site were allowed to move. These residues were: Trp286, Tyr124, Tyr337, Tyr341, Tyr72, Asp74, Thr75, Trp86. The grid box was built with a resolution of 1 Å and 60 × 60 × 72 points and it was positioned at the middle of the protein ($x=116.546$; $y=110.33$; $z=-134.181$). The docking box displayed using ADT constituted a large region to include whole protein target (“blind docking”).

For hBuChE (4BDS) docking calculations were performed following a similar protocol described before for hAChE. Blind dockings were performed by considering a cube of 75 Å³ with grid points spacing of 1 Å positioned at the middle of the protein ($x=137.985$; $y=122.725$; $z=38.78$).

Docking calculations were performed with the programme Autodock Vina³⁶. Default parameters were used except num_modes, which was set to 40.

Molecular docking of compound **14n** into human MAO a/B

Compound **14n** was built as non-protonated amine following the procedure described before for cholinesterases. The crystal structures of human MAO-A in complex with harmine (PDB ID 2Z5X) and human MAO-B crystallised with safinamide (PDB ID 2V5Z) were retrieved from the Protein Data Bank. The enzymes

structures were prepared for docking. First, in the PDB crystallographic structures, any co-crystallised solvent and the ligand were removed. Then, proper bonds, bond orders, hybridisation, and charges were assigned using protein model tool in Discovery Studio, version 2.1, software package, San Diego, CA. CHARMM force field³⁴ was applied using the receptor-ligand interactions tool in Discovery Studio, version 2.1, software package, San Diego, CA. During the protein set up, six water molecules located around the FAD cofactor were considered in the docking experiments because they are essential for stabilising the complexes as also reported in the literature. Finally, atoms of the FAD cofactor were defined in their oxidised state.

The ADT programme was used to generate the docking input files. For MAO-A, the grid centre coordinates were $x=53.065$, $y=161.664$, $z=26.000$ and the size coordinates were $x=24$, $y=34$, $z=38$ with grid points separated 1 Å; for MAO-B, the grid centre coordinates were $x=53.065$, $y=161.664$, $z=29.046$ and the size coordinates were $x=24$, $y=34$, $z=36$ with grid points separated 1 Å.

Docking calculations were performed following the same protocol described before for hAChE.

According to Vina best-scored poses, the most stable complex configurations were considered. The docked ligand output files were viewed and hydrogen bond interactions, van der Waals interactions as well as electrostatic interaction were evaluated using Discovery Studio, San Diego, CA.

Results and discussion

Chemistry

The synthesis of the target compounds **14a–p** was carried out as shown in Scheme 1. The *one-pot* Ugi-4MCR³⁷, with isocyanides **4–7**, (prepared in two steps respectively from tryptamine, 5-methoxytryptamine, isopropoxytryptamine³⁸ and propoxytryptamine³⁸), formaldehyde (**13**), the appropriate commercial amines **8**, **9**, 3-(1-benzylpiperidin-4-yl)propan-1-amine (**10**)³⁹, 4-(1-benzylpiperidin-4-yl)butan-1-amine (**11**)^{39,40}, and 4-oxo-4H-chromene-2-carboxylic acid (**12**), in MeOH/CH₂Cl₂ (3:1) at rt for 24 h, afforded the desired compounds **14a–p** from low to moderate yields. All new compounds showed analytical and spectroscopic

data in good agreement with their structure (see Supplementary Material).

Biological evaluation

The *in vitro* evaluation of compounds **14** started with the analysis of their antioxidant activity, continued with the inhibition of MAO-A and MAO-B and ended with the evaluation of ChEs inhibition.

Antioxidant activity

The antioxidant activity of hybrids **14a–p** was determined by the ORAC-FL method^{30,41}. Results are expressed in relation to radical scavenging properties of Trolox yielding the Trolox equivalents (TE) unit. Ferulic acid and Melatonin were used as positive references molecules showing ORAC values of 3.74¹² and 2.45¹², respectively.

As shown in Table 1 and Figure 2, all compounds presented strong radical scavenging properties with TE values ranging from 2.27 (**14k**) to 6.92 (**14i**). In general, compounds with a length in the linker of $n=1, 2$ are more potent antioxidants than Ferulic acid; however, and except for hybrid **14i**, those with $n=3, 4$ are fewer antioxidants than Ferulic acid, but remain comparable to Melatonin.

In vitro inhibition of human MAOs

Cloroglyline, an irreversible and selective MAOAI and pargyline, an irreversible and selective MAOBI, were used as references. As shown in Table 1, compounds **14a**, **14k**, **14n**, and **14p** can effectively inhibit MAO-A at micromolar range with IC_{50} values equal to 1.99, 2.99, 2.79, and 1.39 μM , respectively, and therefore they are less active than cloroglyline ($IC_{50}=0.05 \mu\text{M}$). Hybrids **14a** and **14p** are selective MAO-AI, while compounds **14k** and **14n** also inhibit MAO-B ($IC_{50}=15.2$ and $21.3 \mu\text{M}$), respectively, and are less potent compared to Pargyline ($IC_{50}=0.08 \mu\text{M}$). Finally, compound **14f** ($IC_{50}=80.59 \mu\text{M}$) is a modest and selective MAOBI.

In vitro inhibition of eeAChE and eqBuChE

To complete the multitarget biological analysis, we analysed the *EeAChE* and *eqBuChE* inhibition, using Donepezil as a reference agent, and the Ellman protocol³² for the determination of enzyme inhibition. As shown in Table 1, the target compounds **14a–p** are generally more active against *eqBuChE* than *EeAChE*. The most effective *eqBuChE* are compounds **14g** ($IC_{50}=6.76 \text{ nM}$) and **14h** ($IC_{50}=6.29 \text{ nM}$), what means that molecules **14g** and **14h** are 133-fold more potent than Donepezil and have an inhibitory potency similar to tacrine. It is worth noting that excluding hybrids **14a–c** and **14m**, the other twelve compounds are potent *BuChE*, in the nanomolar range, showing IC_{50} (nM) values from 6.3 (**14g** and **14h**) to 50.1 (**14i**).

Regarding the structure-activity relationship, and for the same substituent, the most potent inhibitors are those bearing a length in the linker of $n=2$, and the less potent for $n=3, 1$ and 4 , respectively. However, for the same linker length, the most potent compounds are always those bearing propoxy or isopropoxy substituents at the indole ring, such as hybrids **14c,d,g,h,k,l,o,p**.

For the *EeAChE* inhibition, the less potent inhibitors **14a–d** are those with $n=1$ displaying a percentage of inhibition lower than 50% at $10 \mu\text{M}$ concentration, while the three stronger *EeAChE*, showing IC_{50} values ranging from 58.2 (**14m**) to 88.5 nM (**14o**)

correlate with $n=4$ as length in the linker. Compounds **14i–l** with $n=3$ are more potent than hybrids **14e–h** with $n=2$, confirming thus that the inhibition of *EeAChE* increases with the length in the linker. Finally, it is worth of note that compounds **14o–p** are the stronger inhibitors for both *EeAChE* and *eqBuChE*.

In vitro inhibition of hChE

Based on these results, we have selected the most balanced compounds **14a**, **14e–h**, **14k**, **14n**, and **14p**, in terms of the antioxidant properties, MAO-A/B and *EeAChE*/*eqBuChE* inhibitory activities, for the study of the human cholinesterases (hChEs) inhibition. As shown in Table 1, the tested compounds showed higher inhibitory potency against h*BuChE* compared to h*AChE*. The inhibitory activity on h*BuChE* ranges from 11.90 nM (**14n**) to 1167 nM (**14a**), and six of the eight tested compounds (**14e,g,h,k,n**, and **p**) have IC_{50} values under 85 nM; moreover, hybrids **14a** and **14k** are totally selective h*BuChE*. The most potent h*BuChE* is compound **14n**, 70-fold more active than Donepezil and only 2-fold less active than Tacrine. With respect to h*AChE* inhibition, the tested molecules showed IC_{50} values in micromolar range, between 2.62 μM for **14e** and 0.36 μM for the most active compound **14f**, 15-fold less active than Donepezil.

Molecular docking studies

Docking studies were carried out in order to discover the binding modes and the interactions of compound **14n** with h*AChE*, h*BuChE*, hMAO-A, and hMAO-B. Docking simulations and visualisations were performed using AutoDock Vina³⁶ and Discovery Studio, San Diego, CA.

AChE molecular modelling studies

The 3D structure of h*AChE* was retrieved from the PDB (coded as 1B41). Multiple *AChE* X-ray structures have revealed a large mobility of some residues to accommodate ligands. Therefore, the flexibility of eight side chains have been taken into account in docking strategies by allowing side chain flexibility during the docking search as performed by software Autodock Vina³⁶

As shown in Figures 3(a,c), compound **14n** located in the entire enzymatic gorge. Docking simulations showed a clear preference to accommodate the chromone moiety within the PAS while the binding pocket forming the CAS is embedded by the methoxyindole moiety with the flexible linker lying in the middle of the gorge between CAS and PAS.

In the complex, the indole moiety is pointed toward the catalytic triad residues, His447, Ser203, and Glu334 but it does not interact via hydrogen bonding or hydrophobic interactions with any residue of the catalytic triad. It was found that the indole moiety of the ligand is forming $\pi-\pi$ interaction and amide- π stacked interaction with Trp86 and with Gly120, respectively. In addition, the NH and methoxy groups are involved in hydrogen bonds with Glu202 and Ser125, respectively.

The chromone moiety is located in the pocket forming PAS interacting with Tyr124 and Trp286 via face-to-face $\pi-\pi$ stacking interactions. In this situation, the *N*-benzylpiperidinium moiety is turned away from the PAS interacting with Leu289 and Ser293 (Figure 3(b)).

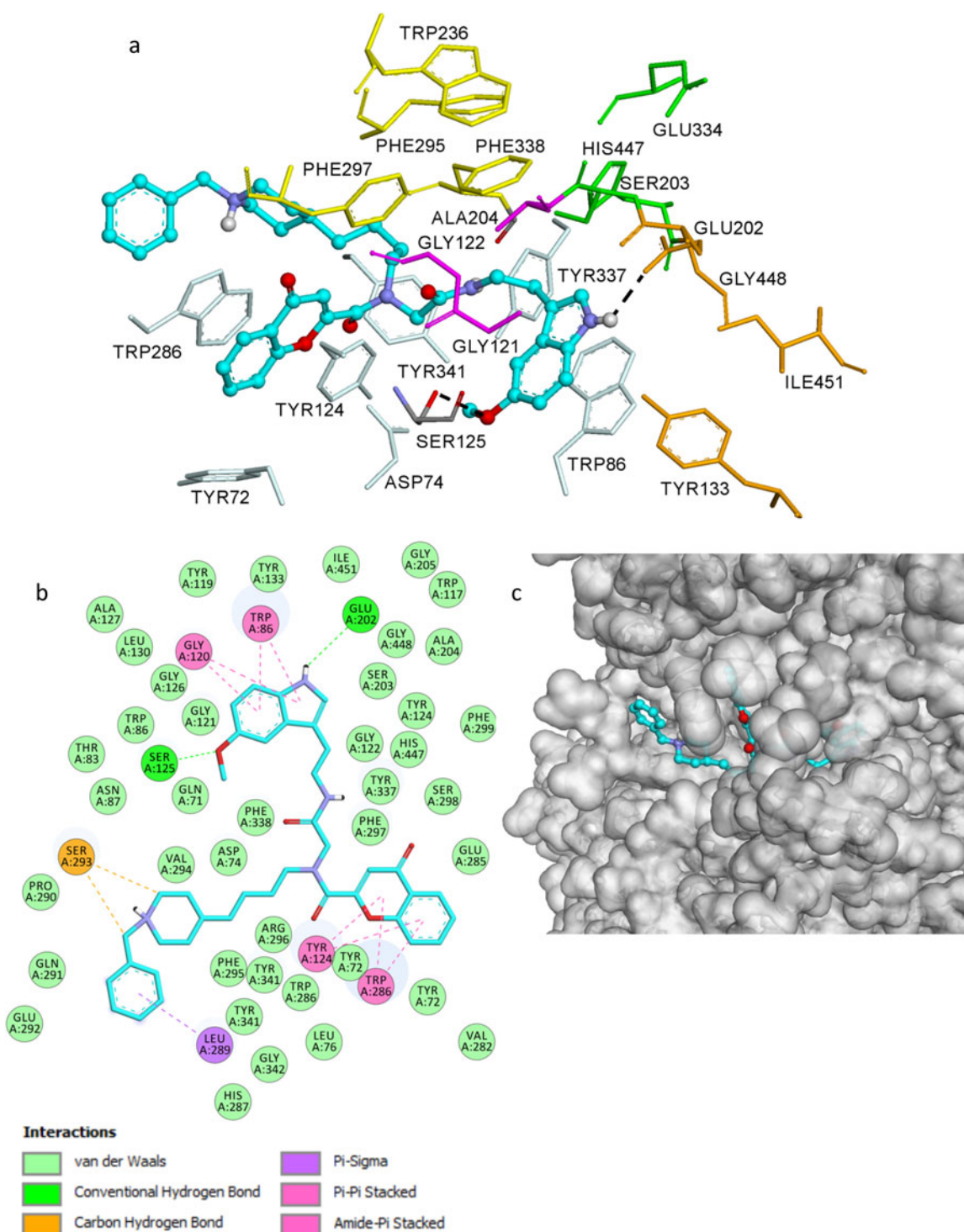


Figure 3. Docked pose of inhibitor **14n** at the active site of hAChE. (a) Compound **14n** is rendered as ball and sticks (carbon atoms in blue) and the side chain conformations of the mobile residues are illustrated in light blue. The catalytic triad (CT) is Coloured in green, the oxyanion hole (OH) in magenta, the anionic sub site (AS) in orange, except Trp86, the acyl binding pocket (ABP) in yellow and PAS in light blue. (b) 2D-representation of interactions established by **14n** with hAChE. (c) 3D surface representation of hAChE (white) with compound **14n** (blue).

BuChE molecular modelling studies

Compound **14n** was modelled into the structure of hBuChE (PDB: 4BDS). The ligand fits into the active site of hBuChE mainly through π - π and hydrogen bonds interactions, which are found to be essential for binding. The binding mode of compound **14n** at the active site of hBuChE is illustrated in Figure 4. The docking results showed that in the lowest energy binding orientation of the ligand, the chromone moiety formed π - π T-shaped interactions with

Phe329 (in the anionic site of the enzyme) and Trp231. The indole moiety binds in the CAS region of the enzyme, establishing π - π stacking interactions with Trp82 and His438 of the catalytic triad.

Besides, the NH group forms a hydrogen bond interaction with His438. The ligand displays additional hydrogen bond interactions between the C=O group of the di-substituted amide with Thr120 and the NH group of the mono-substituted amide with Asp70 in the PAS (Figure 5).

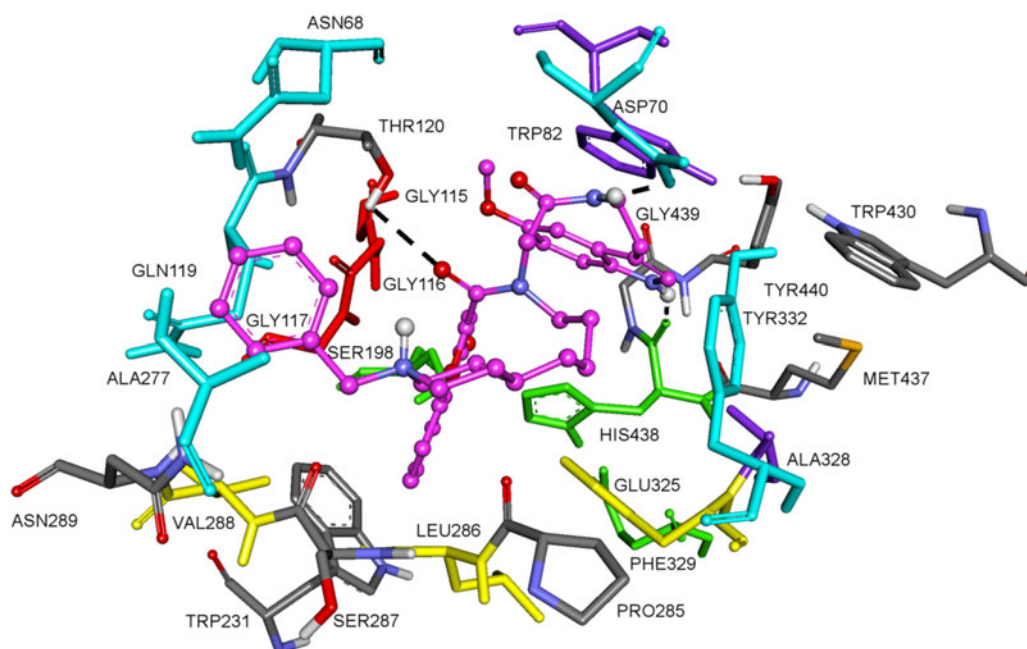


Figure 4. Proposed binding mode for compound **14n** inside gorge cavity of hBuChE. Compound **14n** is Coloured pink. Different subsites of the active site were Coloured: catalytically anionic site (CAS) in green, oxyanion hole (OH) in red, choline binding site (CBS), acyl binding pocket (ABP) in yellow, and peripheral site (PAS) in blue.

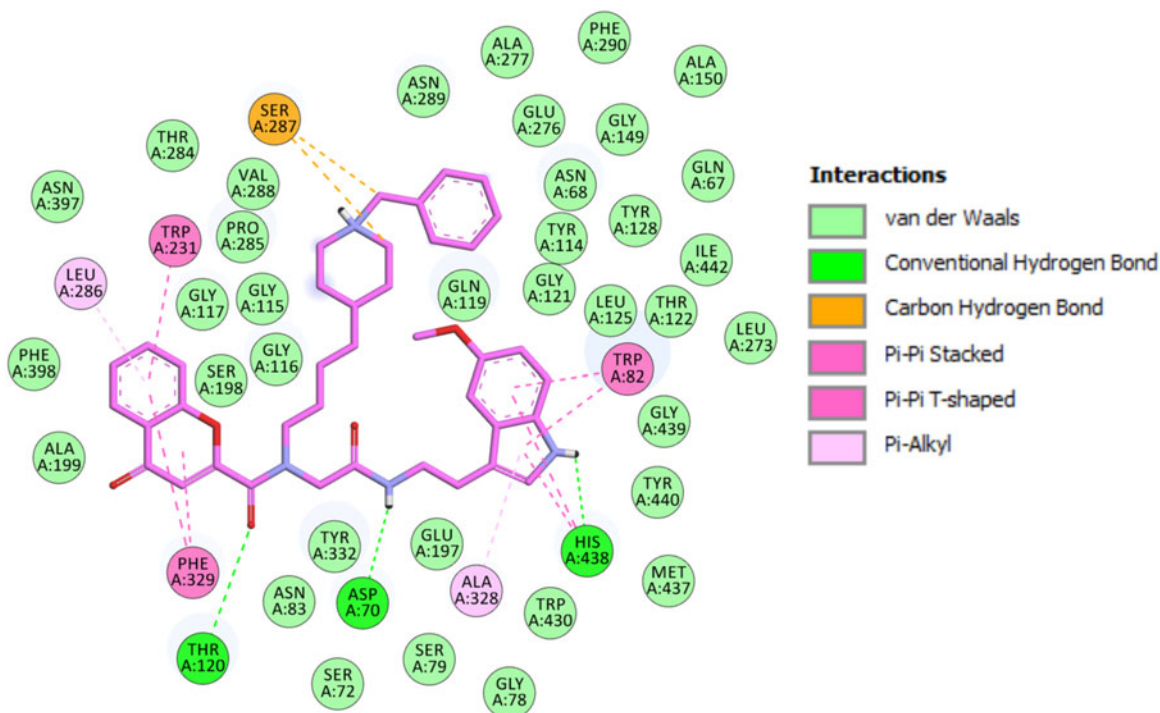


Figure 5. 2D Schematic representation of different interactions of compound **14n** with hBuChE.

Besides the key ligand-enzyme interactions described above, the difference in the AChE and BuChE inhibitory activities may be mainly explained by the inverted orientation adopted by the ligand on both enzymes. It is also noteworthy that for the compound **14n** with three branches, both ending in chromone and indole rings play a key role in the cholinesterase inhibitory activity. The alkyl- *N*-benzylpiperidinium chain placed outside the active site can be important in helping anchor the ligand to the protein.

MAO molecular modelling studies

In order to explore the nature of the ligand-receptor interactions, compound **14n** was docked to the active site of both MAO-A and MAO-B isoforms using the programme Autodock Vina³⁶.

Docking simulations were run on the human model of the MAO-A and MAO-B isoforms. The 3D structures for hMAOs were retrieved from the PDB (PDB ID: 2Z5X for hMAO A and PDB ID: 2V5Z for hMAO B).

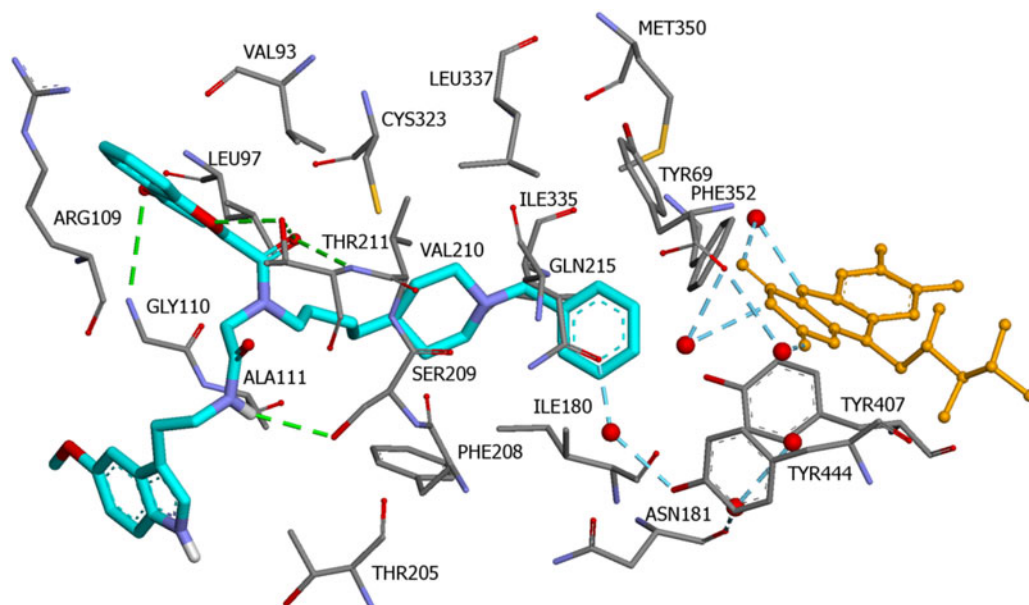


Figure 6. Binding mode of compound **14n** in the active region of hMAO A. Amino acids residues of binding site are colour-coded. The FAD cofactor and the six water molecules represented as an integral part of the MAO-A structure model are rendered as orange balls and sticks and red balls, respectively. Green and blue dashed lines represented hydrogen bond interactions.

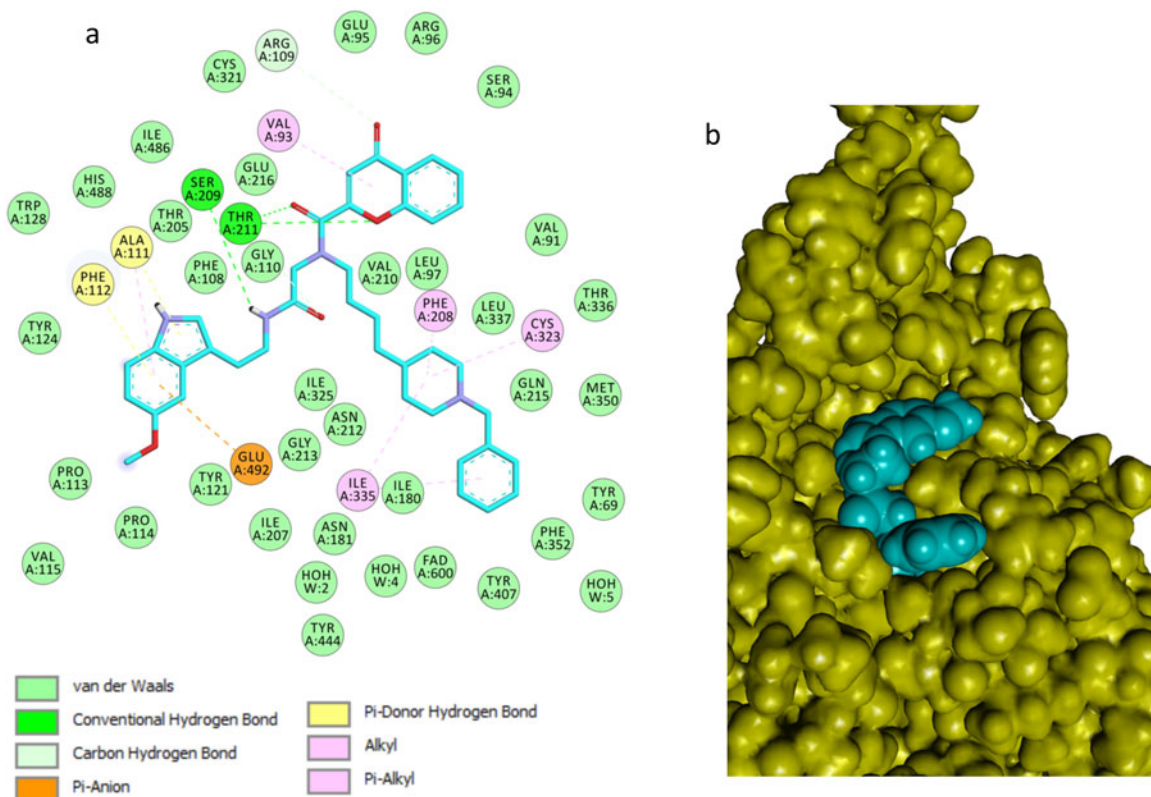


Figure 7. Binding mode of compound **14n** at the binding site of hMAO A. (a) 2D ligand-receptor interaction diagram. (b) Complex of compound **14n** (blue) and hMAO A (yellow).

Results from several studies have shown that it must be the neutral amine that reaches the active site of MAO A and MAO B that allows the chemistry^{42–45}. Based on this fact, the neutral form of **14n** was docked into MAOs enzymes despite that at physiological pH, most of the piperidine rings would be in the protonated, positively charged form.

As reported in our previous papers^{46–48}, six water molecules were considered as integral components of the protein structure in the

docking simulations. These water molecules are labelled as w72, w193, w11, w23, w15, and w53 according to the numbering reported in the hMAO B crystallographic structure (PDB ID: 1S3E) and they are located near the flavin adenine dinucleotide (FAD) cofactor.

Figure 6 illustrates the binding mode of **14n** into the hMAO A binding cavity (binding energy: -8.3 kcal/mol). Visual inspection of the pose of compound **14n** into the MAO-A binding site revealed that the phenyl ring placed in the “aromatic cage” framed by Tyr69,

Phe352, Tyr407, Tyr444 side chains, as well as the isoalloxazine FAD ring. The aromatic ring is oriented to establish π -alkyl interactions with Ile180 residue. The piperidine ring is located in a hydrophobic core delimited by residues Phe208, Ileu335, and Leu337 (Figure 7(a)).

In the entrance cavity, the chromone moiety is located in a hydrophobic core delimited by residues Val93, Leu97, Gly110,

Ala111, and Thr211 (Figure 6). In this orientation, four hydrogen bonds are established, two of them involving the C=O group close to the chromone ring and Thr211; the other two involving the oxygen and the C=O group of the ring and Thr211 and Gly110. Moreover, the NH group of the amide moiety is also able to form a hydrogen bond with Ser209 side chain (Figure 7(a)).

The indole heterocyclic ring did not portray any significant interactions with the MAO-A active site, but it was well accommodated outside in a cleft made up Ala111, Phe112, Pro113, Pro114, Val115, Tyr124, and Glu492 (Figures 7(a,b)).

To rationalise the selectivity of MAO A/B, docking studies of compound **14n** into the MAO B were done. The six structural water molecules selected for hMAO A were also included in the study.

Docking of compound **14n** into the MAO B binding site revealed that this inhibitor also crosses both cavities, presenting the piperidine nucleus located between the "entrance" and "catalytic" cavities, separated by the residues Ile199 and Tyr326 (Figure 8; binding energy: -7.6 kcal/mol). The phenyl ring is oriented toward the bottom of the substrate cavity, interacting with the FAD cofactor as well as Tyr60, Phe343, Gly205, and Tyr398, through van der Waals interactions and π - π interactions. In addition, the chromone moiety was hosted in the large entrance cavity made up by Phe103, Pro104, Trp119, Leu164, Leu167, Phe168, Ile199, and Ileu316. Moreover, the NH amide group formed a hydrogen bond with Glu84. Finally, the indole ring is oriented to the mouth of the entrance cavity in a hydrophobic sub-pocket, which is defined by Pro102, Thr202, Gly101, Arg100, Thr196, and Asn203 (Figure 9(a)).

The different trends regarding the inhibitory activity of **14n** in MAO A and MAO B can be mainly ascribed to the residues that

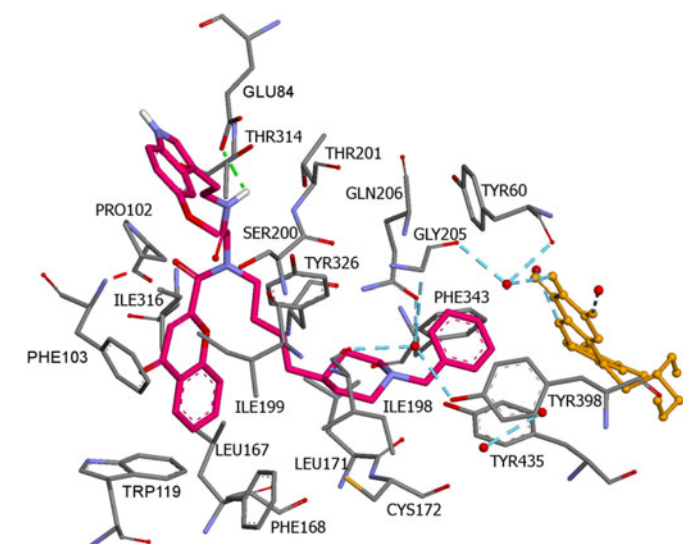


Figure 8. Compound **14n** in the active region of hMAO B. Amino acids residues of binding site are colour-coded. The FAD cofactor and the six water molecules represented as an integral part of the MAO B structure model are rendered as orange balls and sticks and red balls, respectively. Hydrogen bonds are shown with green and blue dashed lines.

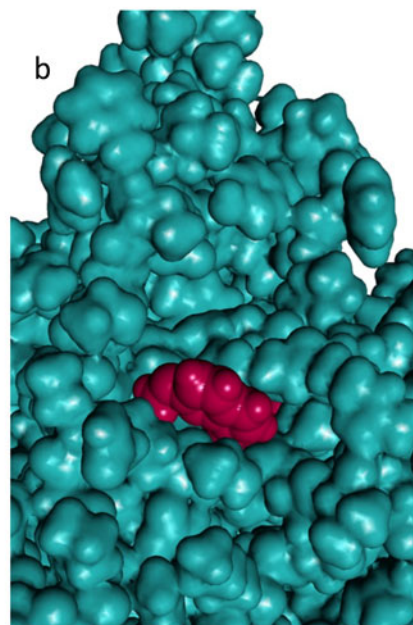
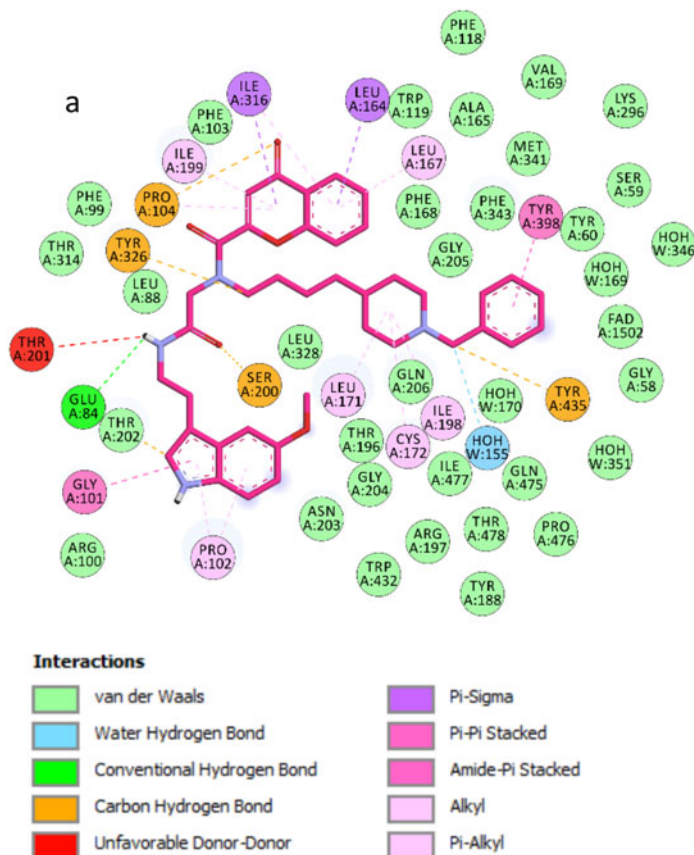


Figure 9. Binding mode of compound **14n** in the active region of hMAO B. Aminoacids residues of binding site are colour-coded. The FAD cofactor and the six water molecules represented as an integral part of the MAO-A structure model are rendered as orange ball and sticks and red balls, respectively. Green and blue dashed lines represented hydrogen bond interactions.

define the bottleneck in the gorge that leads to the ligand binding site. The replacement of Ile199 in MAO B by Phe208 in MAO A pushes slightly the ligand away from the FAD, this cause that it binds more tightly to MAO A and exhibits a greater number of favorable interactions.

In conclusion, the docking simulations have characterised characterised the binding of compound **14n** at the ChE and MAO enzymes. It seems clear that the chains ending in pyrrole and chromone rings are crucial for binding to the active site of the ChEs. However, for MAOs binding is the *N*-benzylpiperidine chain.

Conclusion

In this work, we have described the straightforward Ugi-4MCR synthesis and the biological evaluation of the Donepezil + chromone + melatonin hybrids **14a–p** (Scheme 1, Table 1), as antioxidants, MAOIs, and ChEIs for the potential treatment of AD. From these results, we have identified *N*-(4-(1-benzylpiperidin-4-yl)butyl)-*N*-(2-((2-(5-methoxy-1*H*-indol-3-yl)ethyl)amino)-2-oxoethyl)-4-oxo-4*H*-chromene-2-carboxamide (**14n**), as suitable MTSM for further development. Hybrid **14n** shows strong hBuChE ($IC_{50} = 11.90 \pm 0.05$ nM), moderate hAChE, hMAO A, and MAO-B ($IC_{50} = 1.73 \pm 0.34$ μ M, $IC_{50} = 2.78 \pm 0.12$ μ M, $IC_{50} = 21.29 \pm 3.85$ μ M) inhibition, respectively, while keeping a strong antioxidant effect (3.04 TE).

The inhibition of hybrid **14n** towards BuChE is worth of note, as in patients with moderate to severe forms of AD, AChE activity is decreased, and BuChE, elevated⁴⁹, suggesting that ACh hydrolysis in cholinergic synapses may largely occur *via* BuChE catalysis⁵⁰ and that the specific inhibition of BuChE may be important in raising ACh levels, in order to improve the cognition impairment⁵¹.

To sum up, the present results support the development of new MTSM based on Donepezil + chromone-melatonin hybrids for the potential treatment of AD. This is being investigated in our laboratories and will be reported in due course.

Disclosure statement

No potential conflict of interest was reported by the authors.

Funding

LI thanks the Regional Council of Franche-Comté [2016YC-04540 and 04560] for financial support. JMC and MJOJ thank Universidad Camilo José Cela (UCJC) for support [Grants 2015–12 and 2015–21]. RA and KM were supported by ERDF/ESF project PharmaBrain [no. CZ.02.1.01/0.0/0.0/16_025/0007444] and University of Hradec Kralove [no. IRP1902/2018, VT2201/2018].

ORCID

Kamil Musilek  <http://orcid.org/0000-0002-7504-4062>

Lhassane Ismaili  <http://orcid.org/0000-0002-6013-3150>

References

1. Querfurth HW, LaFerla FM. Alzheimer's Disease. *N Engl J Med* 2010;362:329–44.
2. Bartus RT, Dean RL, Beer B, Lippa AS. The cholinergic hypothesis of geriatric memory dysfunction. *Science* 1982; 217:408–14.
3. Tumiatti V, Minarini A, Bolognesi ML, et al. Tacrine derivatives and Alzheimer's disease. *Curr Med Chem* 2010;17: 1825–38.
4. Rosini M, Simoni E, Milelli A, et al. Oxidative stress in Alzheimer's disease: are we connecting the dots?. *J Med Chem* 2014;57:2821–31.
5. Bush AI. Drug development based on the metals hypothesis of Alzheimer's disease. *J Alzheimers Dis JAD* 2008;15:223–40.
6. Morphy R, Rankovic Z. Designing multiple ligands – medicinal chemistry strategies and challenges. *Curr Pharm Des* 2009;15:587–600.
7. Agis-Torres A, Sollhuber M, Fernandez M, Sanchez-Montero JM. Multi-target-directed ligands and other therapeutic strategies in the search of a real solution for Alzheimer's disease. *Curr Neuropharmacol* 2014;12:2–36.
8. Cavalli A, Bolognesi ML, Minarini A. Multi-target-directed ligands to combat neurodegenerative diseases. *J Med Chem* 2008;51:347–72.
9. León R, Garcia AG, Marco-Contelles J. Recent advances in the multitarget-directed ligands approach for the treatment of Alzheimer's disease. *Med Res Rev* 2013;33:139–89.
10. Oset-Gasque MJ, Marco-Contelles J. Alzheimer's disease, the "one-molecule, one-target" paradigm, and the multitarget directed ligand approach. *ACS Chem Neurosci* 2018;9:401–3.
11. Ismaili L, Refouvelet B, Benchekroun M, et al. Multitarget compounds bearing tacrine- and donepezil-like structural and functional motifs for the potential treatment of Alzheimer's disease. *Prog Neurobiol* 2017;151:4–34.
12. Benchekroun M, Ismaili L, Pudlo M, et al. Donepezil-ferulic acid hybrids as anti-Alzheimer drugs. *Future Med Chem* 2015;7:15–21.
13. Benchekroun M, Romero A, Egea J, et al. The antioxidant additive approach for Alzheimer's disease therapy: new ferulic (lipoic) acid plus melatonin modified tacrines as cholinesterases inhibitors, direct antioxidants, and nuclear factor (erythroid-derived 2)-like 2 activators. *J Med Chem* 2016;59: 9967–73.
14. Ismaili L, do Carmo Carreiras M. Multicomponent reactions for multitargeted compounds for Alzheimer's disease. *Curr Top Med Chem* 2018;17:3319–27.
15. Dömling A, Wang W, Wang K. Chemistry and biology of multicomponent reactions. *Chem Rev* 2012;112:3083–135.
16. Akritopoulou-Zanze I. Isocyanide-based multicomponent reactions in drug discovery. *Curr Opin Chem Biol* 2008;12: 324–31.
17. Biggs-Houck JE, Younai A, Shaw JT. Recent advances in multicomponent reactions for diversity-oriented synthesis. *Curr Opin Chem Biol* 2010;14:371–82.
18. Keri RS, Budagumpi S, Pai RK, Balakrishna RG. Chromones as a privileged scaffold in drug discovery: a review. *Eur J Med Chem* 2014;78:340–74.
19. Gaspar A, Reis J, Fonseca A, et al. Chromone 3-phenylcarboxamides as potent and selective MAO-B inhibitors. *Bioorg Med Chem Lett* 2011;21:707–9.
20. Legoabe LJ, Petzer A, Petzer JP. Selected chromone derivatives as inhibitors of monoamine oxidase. *Bioorg Med Chem Lett* 2012;22:5480–4.
21. Bolasco A, Fioravanti R, Carradori S. Recent development of monoamine oxidase inhibitors. *Expert Opin Ther Pat* 2005; 15:1763–82.
22. Song M-S, Matveychuk D, MacKenzie EM, et al. An update on amine oxidase inhibitors: multifaceted drugs. *Prog Neuropsychopharmacol Biol Psychiatry* 2013;44:118–24.

23. Finberg JPM. Update on the pharmacology of selective inhibitors of MAO-A and MAO-B: focus on modulation of CNS monoamine neurotransmitter release. *Pharmacol Ther* 2014;143:133–52.
24. Li F, Wang Z-M, Wu J-J, et al. Synthesis and pharmacological evaluation of donepezil-based agents as new cholinesterase/monoamine oxidase inhibitors for the potential application against Alzheimer's disease. *J Enzyme Inhib Med Chem* 2016;31:41–53.
25. Zhang H-M, Zhang Y. Melatonin: a well-documented antioxidant with conditional pro-oxidant actions. *J Pineal Res* 2014;57:131–46.
26. Zavadnik IB, Domanski AV, Lapshina EA, et al. Melatonin directly scavenges free radicals generated in red blood cells and a cell-free system: chemiluminescence measurements and theoretical calculations. *Life Sci* 2006;79:391–400.
27. Manchester LC, Coto-Montes A, Boga JA, et al. Melatonin: an ancient molecule that makes oxygen metabolically tolerable. *J Pineal Res* 2015;59:403–19.
28. Masilamoni JG, Jesudason EP, Dhandayuthapani S, et al. The neuroprotective role of melatonin against amyloid β peptide injected mice. *Free Radic Res* 2008;42:661–73.
29. Viegas-Junior C, Danuello A, da Silva Bolzani V, et al. Molecular hybridization: a useful tool in the design of new drug prototypes. *Curr Med Chem* 2007;14:1829–52.
30. Dávalos A, Gómez-Cordovés C, Bartolomé B. Extending applicability of the oxygen radical absorbance capacity (orac – fluorescein) assay. *J Agric Food Chem* 2004;52:48–54.
31. Dgachi Y, Bautista-Aguilera OM, Benchekroun M, et al. Synthesis and biological evaluation of benzochromenopyrimidinones as cholinesterase inhibitors and potent antioxidant, non-hepatotoxic agents for Alzheimer's disease. *Molecules* 2016;21:634.
32. Ellman GL, Courtney KD, Andres V, Featherstone RM. A new and rapid colorimetric determination of acetylcholinesterase activity. *Biochem Pharmacol* 1961;7:88–95.
33. Esquivias-Pérez M, Maalej E, Romero A, et al. Nontoxic and neuroprotective β -naphthotacrines for Alzheimer's disease. *Chem Res Toxicol* 2013;26:986–92.
34. Brooks BR, Bruccoleri RE, Olafson BD, et al. CHARMM: a program for macromolecular energy, minimization, and dynamics calculations. *J Comput Chem* 1983;4:187–217.
35. Morreale A, Maseras F, Iriepa I, Gálvez E. Ligand-receptor interaction at the neural nicotinic acetylcholine binding site: a theoretical model. *J Mol Graph Model* 2002;21:111–8.
36. Trott O, Olson AJ. AutoDock Vina: improving the speed and accuracy of docking with a new scoring function, efficient optimization, and multithreading. *J Comput Chem* 2010;31:455–61.
37. Benchekroun M, Bartolini M, Egea J, et al. Novel tacrine-grafted ugi adducts as multipotent anti-alzheimer drugs: a synthetic renewal in tacrine-ferulic acid hybrids. *ChemMedChem* 2015;10:523–39.
38. Choi JY, Calvet CM, Gunatilleke SS, et al. Rational development of 4-aminopyridyl-based inhibitors targeting trypanosoma cruzi cyp51 as anti-chagas agents. *J Med Chem* 2013;56:7651–68.
39. Bolea I, Juárez-Jiménez J, de los Ríos C, et al. Synthesis, biological evaluation, and molecular modeling of donepezil and N-[(5-(Benzyloxy)-1-methyl-1H-indol-2-yl)methyl]-N-methylprop-2-yn-1-amine hybrids as new multipotent cholinesterase/monoamine oxidase inhibitors for the treatment of Alzheimer's disease. *J Med Chem* 2011;54:8251–70.
40. Mandelli GR, Maiorana S, Terni P, et al. Synthesis of new cardioselective M2 muscarinic receptor antagonists. *Chem Pharm Bull (Tokyo)* 2000;48:1611–22.
41. Ou B, Hampsch-Woodill M, Prior RL. Development and validation of an improved oxygen radical absorbance capacity assay using fluorescein as the fluorescent probe. *J Agric Food Chem* 2001;49:4619–26.
42. Edmondson DE, Mattevi A, Binda C, et al. Structure and mechanism of monoamine oxidase. *Curr Med Chem* 2004;11:1983–93.
43. Jones TZ, Balsa D, Unzeta M, Ramsay RR. Variations in activity and inhibition with pH: the protonated amine is the substrate for monoamine oxidase, but uncharged inhibitors bind better. *J Neural Transm Vienna Austria* 2007;114:707–12.
44. Wang J, Edmondson DE. 2H kinetic isotope effects and pH dependence of catalysis as mechanistic probes of rat monoamine oxidase a: comparisons with the human enzyme. *Biochemistry* 2011;50:7710–7.
45. Scherrer RA, Leo AJ. Multi-pH QSAR: a method to differentiate the activity of neutral and ionized species and obtain true correlations when both species are involved. *Mol Inform* 2010;29:687–93.
46. Samadi A, de los Ríos C, Bolea I, et al. Multipotent MAO and cholinesterase inhibitors for the treatment of Alzheimer's disease: Synthesis, pharmacological analysis and molecular modeling of heterocyclic substituted alkyl and cycloalkyl propargyl amine. *Eur J Med Chem* 2012;52:251–62.
47. Wang L, Esteban G, Ojima M, et al. Donepezil + propargylamine + 8-hydroxyquinoline hybrids as new multifunctional metal-chelators, ChE and MAO inhibitors for the potential treatment of Alzheimer's disease. *Eur J Med Chem* 2014;80:543–61.
48. Bautista-Aguilera OM, Esteban G, Bolea I, et al. Design, synthesis, pharmacological evaluation, QSAR analysis, molecular modeling and ADMET of novel donepezil-indolyl hybrids as multipotent cholinesterase/monoamine oxidase inhibitors for the potential treatment of Alzheimer's disease. *Eur J Med Chem* 2014;75:82–95.
49. Arendt T, Brückner MK, Lange M, Bigl V. Changes in acetylcholinesterase and butyrylcholinesterase in Alzheimer's disease resemble embryonic development—a study of molecular forms. *Neurochem Int* 1992;21:381–96.
50. Darvesh S, Hopkins DA, Geula C. Neurobiology of butyrylcholinesterase. *Nat Rev Neurosci* 2003;4:131–8.
51. Greig NH, Utsuki T, Ingram DK, et al. Selective butyrylcholinesterase inhibition elevates brain acetylcholine, augments learning and lowers Alzheimer beta-amyloid peptide in rodent. *Proc Natl Acad Sci USA* 2005;102:17213–8.